

# Equilibrium magnetization configurations in helical magnets

Ot Garcés Ortiz\*

*Dept. Física de la Matèria Condensada, Univ. de Barcelona, Diagonal 647, 08028 Barcelona, Spain.*

Advisor: Òscar Iglesias Clotas

We have taken an in-depth study of curvature effects on the magnetism of low dimensional nanostructures. We present a general theoretical framework based on a continuous approach to the micromagnetic relevant energy terms (exchange and anisotropy). The model shows that curvature induces effective anisotropy and Dzyaloshinskii-Moriya interactions that are not present in conventional cases. We have particularized the study to helical ferromagnetic helices, and found that they exhibit stable magnetization transitions between quasi-tangential to onion-like configurations. By performing atomistic Monte Carlo simulations, we have validated the theoretical framework and obtained a phase diagram of both phases. We have also performed MC simulations considering only dipolar interactions and found that abrupt magnetic ground state configuration transitions can be induced. Calculations are detailed in [1].

## I. INTRODUCTION

The role that geometry and topology play in emergent order parameters has become an important topic in theoretical and experimental studies in different areas of physics. It has been shown that the geometry of the underlying substrate plays an important role in fields such as liquid crystals [2], fluid flows [3], domain wall dynamics [4], geometrical band theory [5] or superconductors [6]. The effects of curvature on magnetic structures have been studied in a broad variety of low dimensional systems including spherical shells, Möbius strips and double helices [7]. A general theoretical framework to describe statics and dynamics of curved magnetic wires and surfaces has been developed recently, providing a starting point to study magnetization configurations in curvilinear structures [8]. As we will see, the model applies concepts of differential geometry to rewrite the relevant energy terms describing a magnetic material in the continuum micromagnetic approach. When the total energy is written in local curvilinear coordinates, new terms such as induced effective anisotropies and emergent Dzyaloshinskii-Moriya (DM) interactions appear as a consequence of curvature, which are responsible for magnetochiral effects not present in the conventional cases. Advances in materials fabrication have made it possible to synthesize these kinds of systems at submicrometric scales [9], which has enabled the study of magnetization patterns in curved geometries [10] and has paved the way to the emergence of alternative data storage [11] and sensing [12] technologies based on curvature effects.

## II. THEORETICAL FRAMEWORK

The description of magnetization statics and dynamics in the continuum limit focuses on the energy functional of the system, which at least has to include the exchange

interactions and anisotropy energies. As we will consider only ferromagnetic (FM) materials with uniaxial anisotropy, our starting point will be the following basic energy functional for the classical Heisenberg model [8]

$$\mathcal{E} = \int_{\Omega} dV \left[ \ell^2 \mathcal{E}_{\text{ex}} + \lambda (\mathbf{m} \cdot \mathbf{e}_{\text{an}})^2 \right], \quad (1)$$

where the first term is the isotropic exchange interaction, being  $\ell = \sqrt{A/4\pi M_s^2}$  the exchange length,  $A$  the exchange stiffness,  $M_s$  the saturation magnetization and  $\mathbf{m}$  the normalized magnetization  $\mathbf{m} = \mathbf{M}/M_s$ . The second term is the anisotropy energy, being  $\mathbf{e}_{\text{an}}$  a unit vector pointing along the anisotropy axis and  $\lambda$  a dimensionless anisotropy constant.

We will now particularize the previous expression to the case of a curved wire, thin enough so that we can assume that its transverse dimensions are smaller than magnetic characteristic length  $w \equiv \ell/\sqrt{|\lambda|}$ , and that the magnetization is uniform along its cross-section. We can generate the generally curved wire by the curve  $\gamma(s)$  in  $\mathbb{R}^3$ , which will be parametrized by the arc length  $s$ . To ease the description of the magnetic behaviour of the wire, it turns useful to make a transformation to the Frenet-Serret (FS) frame that follows the geometry of the material. Its basis vectors can be computed as

$$\mathbf{e}_1(s) = \gamma'(s), \quad \mathbf{e}_2(s) = \frac{\gamma''(s)}{|\gamma''(s)|}, \quad \mathbf{e}_3(s) = \mathbf{e}_1(s) \times \mathbf{e}_2(s), \quad (2)$$

being  $\mathbf{e}_1(s)$  the tangent,  $\mathbf{e}_2(s)$  the normal and  $\mathbf{e}_3(s)$  the binormal vectors (see schematic drawing in Fig. 1). The relation of the FS frame and its basis derivatives with respect to the parameter  $s$  is given by the FS formulas, which will be used to express the isotropic exchange density on the FS frame. These formulas are  $\mathbf{e}'_{\alpha} = \mathcal{F}_{\alpha\beta} \mathbf{e}_{\beta}$  where  $\mathcal{F}_{\alpha\beta}$  are the components of

$$\mathcal{F} = \begin{pmatrix} 0 & \kappa(s) & 0 \\ -\kappa(s) & 0 & \tau(s) \\ 0 & -\tau(s) & 0 \end{pmatrix} \quad (3)$$

---

\*e-mail address: [otgarces@gmail.com](mailto:otgarces@gmail.com)

where  $\kappa(s)$ ,  $\tau(s)$  are the curvature and torsion of the curve  $\gamma(s)$ , respectively. In order to parametrize the wire, we define two more variables  $\xi_1$ ,  $\xi_2$  such that  $\xi_1 \in [-l_1/2, l_1/2]$ ,  $\xi_2 \in [-l_2/2, l_2/2]$  being  $l_1, l_2 \ll w$ , so that we can assume that the magnetization is uniform along the cross-section of the wire. The space domain of the curved wire is defined as

$$\mathbf{r}(s; \xi_1, \xi_2) = \gamma(s) + \xi_1 \mathbf{e}_2(s) + \xi_2 \mathbf{e}_3(s). \quad (4)$$

We can formalize the one-dimensionality of the magnetization as  $\mathbf{m} = \mathbf{m}(s)$ . We can also assume that  $l_1, l_2 \ll 1/\kappa(s)$ ,  $1/\tau(s)$  for the wire to be sufficiently smooth.

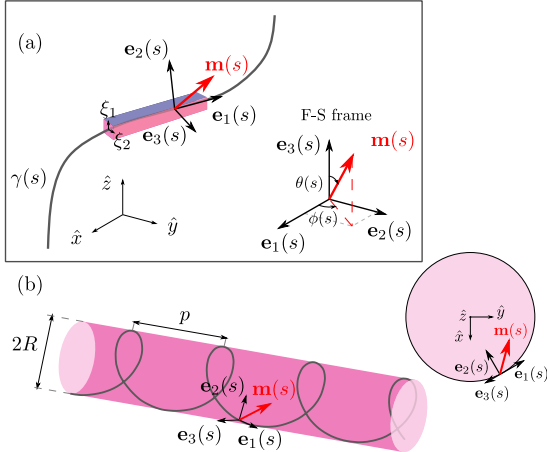


FIG. 1: (a) Space domain of the curved wire and the local magnetization  $\mathbf{m}(s)$ . (b) Scheme showing the configuration of the helical wire, its defining parameters  $R, p$ , and the FS frame drawn from upper and perspective views.

With these assumptions, Eq. (1) can be simplified as we can separate the volume integral into a surface integral that evaluates to the cross-section area  $\mathcal{S} \equiv l_1 l_2$  and the integration along the parameter  $s$

$$\mathcal{E} = \mathcal{S} \int_{\Omega_s} ds \left[ \ell^2 \mathcal{E}_{\text{ex}}(s) + \lambda (\mathbf{m}(s) \cdot \mathbf{e}_{\text{an}}(s))^2 \right]. \quad (5)$$

The aim now is to express the energy functional in the local FS frame. The second term of the energy functional in Eq. (5) can be trivially expressed in the FS frame if  $\mathbf{e}_{\text{an}}(s)$  points along one of the FS frame basis directions, which is the case of interest. In the cartesian frame, the exchange energy density simply reads

$$\mathcal{E}_{\text{ex}} = (\nabla m_i) (\nabla m_i). \quad (6)$$

so that in the curvilinear FS frame, we replace  $\nabla \equiv \mathbf{e}_1(s) \partial_s$  and the magnetization cartesian components by  $m_i = \hat{\mathbf{x}}_i \cdot (\mathbf{e}_\alpha m_\alpha)$ . Then, we can rewrite Eq. (6) as

$$\mathcal{E}_{\text{ex}} = (m_\alpha(s) \mathbf{e}_\alpha(s))' \cdot (m_\beta(s) \mathbf{e}_\beta(s))'. \quad (7)$$

Expanding now this expression, one can show that the exchange energy density separates into three different

terms

$$\mathcal{E}_{\text{ex}} = \mathcal{E}_{\text{ex}}^0 + \mathcal{E}_{\text{ex}}^{\text{A}} + \mathcal{E}_{\text{ex}}^{\text{DM}}. \quad (8)$$

The first term,  $\mathcal{E}_{\text{ex}}^0$  has the shape of the usual form of isotropic exchange energy density for a straight wire. The second term is an effective anisotropy energy density, which, as shown in [Supp. Mat. \[1\]](#), depends on the components of a tensor  $\mathcal{H}_{\alpha\beta}$  that is a bilinear form acting on the magnetization in the curvilinear frame. The third term can be interpreted as an effective DM interaction that mixes components and derivatives of  $\mathbf{m}(s)$ , corresponding to the symmetry of local chiral interactions in the form of Lifshitz invariants  $\mathcal{L}_{ij}^X = m_i \partial_\chi m_j - m_j \partial_\chi m_i$ . The tensor components ruling this effective antisymmetric exchange interaction are just the FS tensor coefficients  $\mathcal{F}_{\alpha\beta}$ .

To derive the equations governing the magnetization dynamics of the nanowire, we parametrize the unit vector  $\mathbf{m}(s)$  in spherical angles  $\theta(s)$  and  $\phi(s)$ .

$$\mathbf{m}(s) = \cos \phi \sin \theta \mathbf{e}_1(s) + \sin \phi \sin \theta \mathbf{e}_2(s) + \cos \theta \mathbf{e}_3(s). \quad (9)$$

with  $\theta, \phi$  characterizing deviations from the binomial and tangent directions. After performing some tedious algebra operations (see [Supp. Mat. \[1\]](#)), the exchange energy density  $\mathcal{E}_{\text{ex}}$  can be written as follows

$$\mathcal{E}_{\text{ex}} = [\theta' - \tau \sin \phi]^2 + [\sin \theta (\phi' + \kappa) - \tau \cos \theta \cos \phi]^2 \quad (10)$$

Since the main interest in this work is on static magnetic equilibrium configurations, we are led to find  $\theta(s)$  and  $\phi(s)$  which minimize the total energy functional. That is, solving the differential system of equations

$$\frac{\delta \mathcal{E}}{\delta \theta} = 0, \quad \frac{\delta \mathcal{E}}{\delta \phi} = 0. \quad (11)$$

### III. EQUILIBRIUM CONFIGURATIONS OF FM HELICES

We will now focus on the study of curvature effects in a FM helix, since this kind of nanostructures have been synthesized and its magnetic properties reported in some studies [13]. Moreover, the helix has constant curvature  $\kappa$  and torsion  $\tau$ , which makes analytic calculations more tractable. Also, we will only consider the case of easy tangential anisotropy, for which  $\lambda < 0$  and  $\mathbf{e}_{\text{an}}(s) \equiv \mathbf{e}_1(s)$  so that  $\mathcal{E}_{\text{an}} = -|\lambda| \sin^2 \theta \cos^2 \phi$ .

The parametrization of the helix wire (see Fig. 1 (b)) can be done in terms of the helix radius  $R$  and pitch  $2\pi p$  using the arc length  $s$  as a parameter as:

$$\gamma(s) = \left( R \cos \frac{s}{\tilde{s}}, R \sin \frac{s}{\tilde{s}}, p \frac{s}{\tilde{s}} \right) \quad (12)$$

where  $\tilde{s} = 1/\sqrt{\kappa^2 + \tau^2}$ . Its curvature and torsion can be computed as  $\kappa = R/(R^2 + p^2)$  and  $\tau = p/(R^2 + p^2)$ .

In order to find the equilibrium states of the helix, it is convenient to rewrite the energy functional of Eq. (5) in terms of a scaled variable  $\chi \equiv s/\tilde{s}$ , as detailed in [Supp. Mat.](#) [1]. The differential equations governing  $\theta(s)$  and  $\phi(s)$  are obtained applying the functional equations Eq. (11). This results in the following coupled system of differential equations for  $\theta(s)$  and  $\phi(s)$

$$\begin{aligned} \partial_s^2 \theta + \tau \cos \phi [\kappa \cos 2\theta - 2\partial_s \phi \sin^2 \theta] \\ - \cos \theta \sin \theta [(\partial_s \phi + \kappa)^2 - \tau^2 \cos^2 \phi] \\ + w^{-2} \sin \theta \cos \theta \cos^2 \phi = 0 \end{aligned} \quad (13)$$

$$\begin{aligned} \sin^2 \theta [\partial_s^2 \phi + 2\tau \partial_s \theta \cos \phi - \tau^2 \cos \phi \sin \phi] \\ + \cos \theta \sin \theta [2\partial_s \theta (\partial_s \phi + \kappa) - \kappa \tau \sin \phi] \\ - w^{-2} \cos \phi \sin \phi \sin^2 \theta = 0. \end{aligned} \quad (14)$$

### A. Quasi-tangential configurations.

A hint to the particular solution of the previous system of equations can be found considering a ring shaped wire, for which planar vortex states (homogeneous solutions in the FS frame with constant  $\phi$  and  $\mathbf{m}$  pointing strictly in the tangential direction) were reported in [8]. Since the helix has constant  $\kappa$ ,  $\tau$ , we may expect that in the limit of small  $\kappa$  and  $\tau$  the configurations will be described by the so-called quasi-tangential (QT) state, characterized by the 'ansatz'  $\phi(s) = 0, \pi$  with the corresponding (anti)clockwise chiralities  $\mathcal{C} \equiv \cos \phi = (-1) + 1$ . Setting  $\phi(s) = 0, \pi$  in Eqs. (13) & (14) simplifies the equations to

$$\begin{cases} \tau \kappa \mathcal{C} \cos 2\theta + w^2 \partial_s^2 \theta + \sin \theta \cos \theta (1 - \kappa^2 + \tau^2) = 0 \\ \partial_s \theta (\kappa^2 \sin 2\theta + 2\tau \kappa \mathcal{C} \sin^2 \theta) = 0, \end{cases} \quad (15)$$

where we defined  $\kappa \equiv w\kappa$ ,  $\tau \equiv w\tau$  as the reduced curvature and torsion respectively. Setting then  $\theta$  independent of  $s$ , Eqs. (15) can be easily solved to find

$$\tan 2\theta_{\text{QT}} = -\frac{2\mathcal{C}\kappa\tau}{1 - \kappa^2 + \tau^2}, \quad \phi_{\text{QT}} = 0, \pi. \quad (16)$$

Using double angle formulas for the tangent one can find a closed expression for  $\theta_{\text{QT}}$

$$\theta_{\text{QT}}(\kappa, \tau) = \frac{\pi}{2} - \arctan \left( \frac{2\mathcal{C}\kappa\tau}{\zeta + \sqrt{\zeta^2 + 4\kappa^2\tau^2}} \right) \quad (17)$$

where  $\zeta \equiv 1 - \kappa^2 + \tau^2$ . This corresponds to a configuration where the magnetization deviates from the local tangent vector  $\mathbf{e}_1(s)$  by a constant angle  $\theta_{\text{QT}}$  which depends on the chirality  $\mathcal{C}$  and the reduced curvature and torsion  $\kappa$ ,  $\tau$ , as can be seen in Fig. 2. Therefore, even in the high anisotropy case, magnetization will always deviate from the tangential direction due to curvature effects.

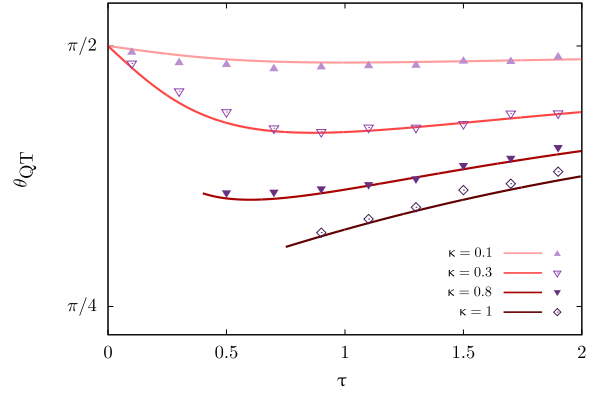


FIG. 2: Angle characterizing the deviation of  $\mathbf{m}(s)$  from the tangent direction  $\mathbf{e}_1$  of the QT stable configurations as a function of  $\tau$  for different values of  $\kappa$  and  $\mathcal{C} = +1$  as given by Eq. (17) (continuous lines). Points correspond to simulation results for values of  $\tau$  down to where the limit of stability of the QT phase is observed.

In analogy with the case of the ring shaped wire [8], one expects this homogeneous QT solution to be valid in the case of small  $\kappa, \tau$ . In fact, in this case the configuration becomes purely tangential as can be seen in Fig. 2, and in this case we can approximate Eq. (17) to first order in  $\kappa$  and  $\tau$  as

$$\theta_{\text{QT}} \simeq \frac{\pi}{2} - \mathcal{C}\tau\kappa, \quad \kappa, \tau \ll 1 \quad (18)$$

This approximate solution is plotted in Fig. 2 as a function of  $\tau$  for wires with different curvatures up to its limits of validity and agrees surprisingly well with the values extracted from the configurations obtained from simulations to be described in the next Sec. III C (symbols in Fig. 2).

Whereas for a ring shaped wire (corresponding to  $\tau \rightarrow 0$ ) [8], a transition from a *vortex state* at low  $\kappa$  to a so-called *onion state* is observed for  $\kappa > \kappa_0$  ( $\kappa_0 \approx 0.657$ ), we would expect that for larger  $\kappa, \tau$  the equilibrium configurations of the helix wire change from the QT state (with homogeneous  $\theta$ ) to an onion state characterized by a periodic variation of  $\theta_{\text{OS}}(s)$  and  $\phi_{\text{OS}}(s)$  in the FS frame.

### B. Onion state configurations.

For larger  $\kappa, \tau$ , we need to find solutions different from the QT 'ansatz' used before. The natural parametrization of the helix is implemented through the scaled coordinate  $\chi = s/\tilde{s}$ . In analogy to the case of the ring shaped wire [8], we are looking for  $2\pi$ -periodic (with respect to  $\chi$ ) solutions of the set of equations Eqs. (13) & (14), that can be written in the form

$$\theta_{\text{OS}}(\chi) = \sum_{n=0}^{\infty} \alpha_n \cos n\chi + \beta_n \sin n\chi \quad (19)$$

$$\phi_{\text{OS}}(\chi) = \sum_{n=0}^{\infty} \tilde{\alpha}_n \cos n\chi + \tilde{\beta}_n \sin n\chi \quad (20)$$

Now, solutions must be found numerically for  $\alpha_n, \beta_n, \bar{\alpha}_n, \bar{\beta}_n$  by directly substituting these  $2\pi$ -periodic expansions into these equations.

### C. Simulations

To check the validity of the analytical results for the continuous micromagnetic model, we performed computer Monte Carlo (MC) simulations using the Metropolis algorithm to search for minimum energy configurations using a simulated annealing process from a high temperature disordered state down to low temperature. We have implemented an atomistic, discretized version of the continuous model presented above, considering Heisenberg spins  $\mathbf{s}_i$  distributed along helical chain with uniform density and with energy given by a lattice version of Eq. 5.

The model discussed above has been implemented setting the atomistic exchange constant  $J = 1$  and the anisotropy constant  $K = 1$  such that  $w = 1$  in the continuum model. In this way, we can control the parameters  $\kappa, \tau$  by setting the values of  $\kappa, \tau$ . We have performed simulations for a wide range of values of  $\kappa, \tau$  to establish the phase diagram for the two possible magnetization configurations as presented in Fig. 3: (a) QT phase as presented in Subsec. III A, which is generally found for smaller values of  $\kappa, \tau$  and (b) onion state as presented in Subsec. III B, generally found for larger values of  $\kappa, \tau$ .

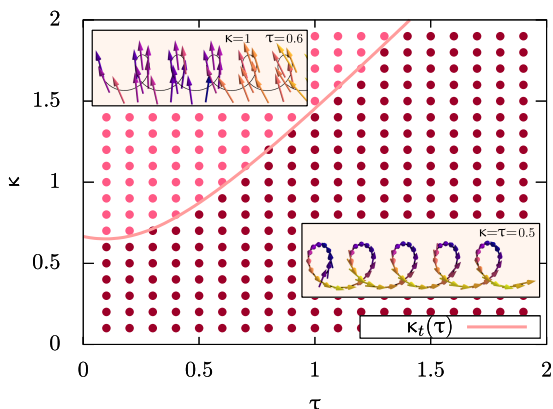


FIG. 3: Phase diagram of stable magnetization configurations in the helix wire as obtained by MC simulations. Dark red dots correspond to QT states as exemplified in the lower inset. Pink dots correspond to onion state as shown in the upper inset. The thick line  $\kappa_t(\tau)$  signals the boundary between both phases.

To establish the phase diagram, we have used the order parameter  $\eta \equiv \langle \theta \rangle - \theta_{QT}(\kappa, \tau)$ , where  $\langle \theta \rangle$  is calculated from the simulated configurations and  $\theta_{QT}(\kappa, \tau)$  is given by Eq. (17). Therefore, for a given  $\kappa$ , we have gathered the  $\tau$  at which the transition from  $\eta \approx 0$  for QT to  $\eta \neq 0$  for onion-like states is observed. The continuous boundary line  $\kappa_t(\tau)$  separating both phases represented in Fig. 3 has been obtained by fitting a curve to the points mentioned before. The results are presented in Fig. 3.

### IV. DIPOLAR HELICAL WIRES

Within the theoretical framework presented in previous sections, only on-site and nearest neighbour (n.n.) interactions could be incorporated. We considered that dipolar interactions (DI) were weak and could be accounted as an additional effective anisotropy. However, assemblies of nanoparticles, magnetic beads or molecular clusters, can be treated as magnetic macro-dipoles whose magnetic order is dominated by the long-range DI between them [14]. At difference from exchange coupling, DI depend also on the distance and are highly anisotropic in space. In particular, they favour FM alignment of dipoles placed head-to-head and AF alignment if they are side-by-side. In Sec. III, we showed that magnetic states can be tuned by varying  $\tau, \kappa$  which depend on material parameters (included in  $w$ ). However, we expect that in dipolar helices (see Fig. 4(b)) magnetic states can be controlled also by tuning the angle between consecutive dipoles  $\varphi$  that determines the n.n. distance  $r_{nn}$ , apart from the more natural parameters  $R, p$ .

To show this, we have performed MC simulations to find the ground state magnetic configurations of a discrete model of a dipolar helix by considering  $N_a$  magnetic dipoles  $\mathbf{m}_i = \mu_i \mu_B \mathbf{s}_i$  arranged as shown in Fig. 4(b) and interacting solely through magnetic dipolar interactions described with the following energy

$$\mathcal{E}_{\text{dip}}^s = g_{\text{dip}} \sum_{i,j=1}^{N_a} \mu_i \mu_j \left[ \frac{\mathbf{s}_i \cdot \mathbf{s}_j}{r_{ij}^3} - 3 \frac{(\mathbf{s}_i \cdot \mathbf{r}_{ij})(\mathbf{s}_j \cdot \mathbf{r}_{ij})}{r_{ij}^5} \right], \quad (21)$$

where  $\mathbf{r}_{ij}$  is the relative position vector joining the sites of spins  $\mathbf{s}_i$  and  $\mathbf{s}_j$ ,  $\mu_i$  is the atomic magnetic moment in units of the Bohr magneton  $\mu_B$ , and  $g_{\text{dip}} = \mu_0 \mu_B^2 / 4\pi a^3$  is the dipolar strength,  $\mu_0$  is the absolute permeability and  $a$  the lattice constant.

In Fig. 4, we show the staggered averaged projection of the magnetization  $\langle |m_z| \rangle$  of configurations obtained for an helix with  $R = 1$  and  $p = \pi/2$  as a case example. As it can be seen in the insets, a wide variety of magnetic orders can be achieved by varying  $\varphi$ . For high  $p$  and small  $\varphi$  (high density), we obtain QT states as those shown in subpanels (i), (ii). In this regime, the n.n. of a dipole are the immediate preceding and next along the helix, and  $r_{nn}$  varies linearly with  $\varphi$ . Below some critical  $p$ ,  $r_{nn}(\varphi)$  starts to show oscillatory behaviour above some value of  $\varphi$  at which  $r_{nn} > p$  and the n.n. of a given dipole are found at different helix turns, instead of being the ones contiguous to it. This explains the formation of AF states such as (iii), (v), (vi), (viii) with entwined head-to-tail magnetic helices that have a periodicity different from the generative helix. The number of magnetic helices changes at values of  $\varphi$  such that a maximum in  $r_{nn}(\varphi)$  coincides with a minimum in  $r_{nnn}(\varphi)$ . At these points, AF straight chains such as those shown in (iv) and (vii) are formed.

These abrupt changes in the magnetic order of the di-

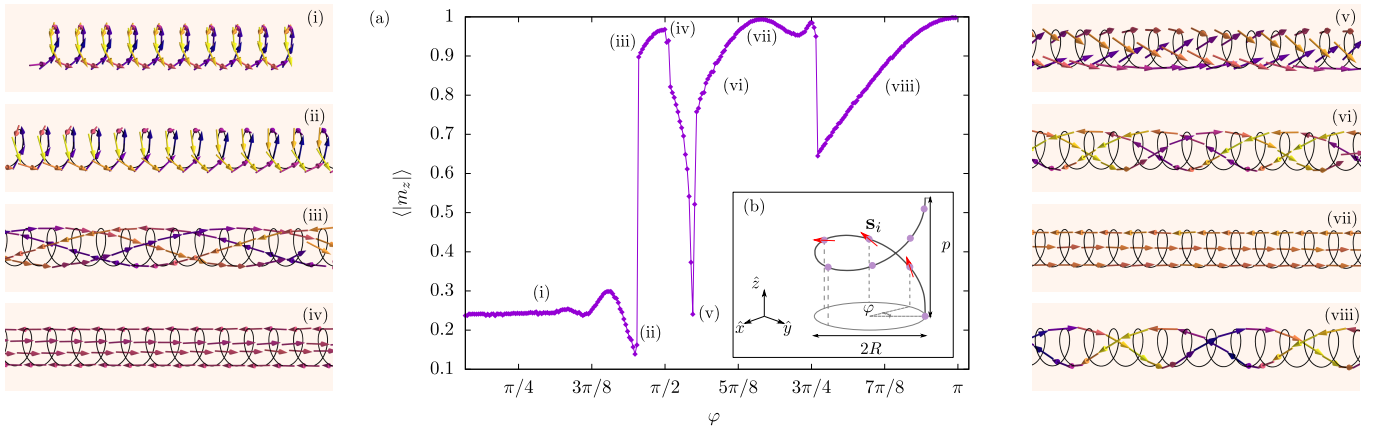


FIG. 4: Results of the lowest energy configurations obtained by MC simulations in dipolar helix containing  $N = 100$  dipoles with  $p = \pi/2$ , and  $R = 1$  as a function angle  $\varphi$ . In main panel (a) we display the absolute value of the magnetization component along the helix axis averaged over the helix sites. Inset (b) shows a representation of the parameters defining the dipolar helices. Subpanels (i) to (viii) display low temperature spin configurations achieved after a simulated annealing of representative values of  $\varphi$  indicated in panel (a).

polar helices can also be induced by varying  $p$ , as can be seen in Fig. 5. Assuming that  $\varphi$  does not vary significantly when producing small changes in  $p$ , we can switch stable magnetic configurations from  $\langle |m_z| \rangle \approx 0$  to  $\langle |m_z| \rangle \approx 1$ . This way, we can induce magnetization configuration transitions by applying mechanical stress to the magnetic helix. These effects have already been studied and directed towards the field of magneto-mechanical response of magnetic materials and stress sensing using these magnetic materials [7].

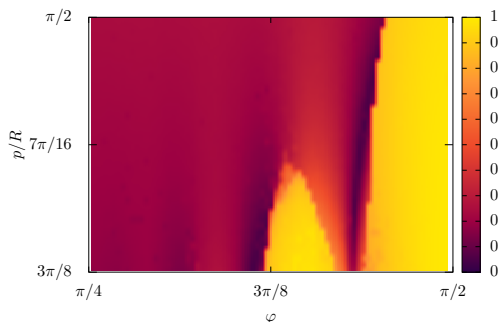


FIG. 5: Heatmap showing  $\langle |m_z| \rangle$  for ground state configurations obtained for a range of angles  $\varphi$  and pitches  $p/R$ .

## V. CONCLUSIONS

Firstly, we have studied the technical details of the continuous micromagnetic model in curved geometries pre-

sented in [8] including detailed explanations and calculations. In order to check the validity of the model, we have focused on FM helices. A theoretical study of the particular geometry of the helix has also been provided, for which equations governing the magnetization statics have been derived. When studying their analytical solutions, we have found a phase transition between two stable magnetization states: almost tangential or QT for small  $\kappa, \tau$  and QT or *onion state* for larger  $\kappa, \tau$ . With the help of MC simulations we have obtained a phase diagram and validated the theoretical framework.

In the second part of the study, we have found that, when considering only DI, magnetic ground state configurations can be controlled by means of varying the natural parameters of the helix,  $R, p$ , and the angle between contiguous dipoles  $\varphi$ . We have also found that we can induce abrupt magnetic configuration transitions when mechanical stress is applied to the helix.

## Acknowledgments

I would like to foremost thank Dr. Òscar Iglesias for the guidance and help to carry on with this work. I am also thankful for the help and support received from family and friends throughout all these years. We thank CSUC for computational resources.

- [1] O. Garcés and O. Iglesias, [10.5281/zenodo.6617294](https://zenodo.org/record/6617294).
- [2] A. R. Fialho *et al.*, *Phys. Rev. E* **95**, 012702 (2017).
- [3] P. Rajbanshi *et al.*, *Phys. Rev. Fluids* **3**, 024201 (2018).
- [4] K. V. Yershov *et al.*, *Phys. Rev. B* **98**, 060409 (2018).
- [5] J. Cayssol *et al.*, *J. Phys.: Mater.* **4**, 034007 (2021).
- [6] J. Tempere *et al.*, *Phys. Rev. B* **79**, 134516 (2009).
- [7] D. D. Sheka *et al.*, *Small* **18**, 2105219 (2022).
- [8] D. D. Sheka *et al.*, *J. Phys. A Math. Theor.* **48**, 125202

- (2015).
- [9] D. P. Weber *et al.*, *Nano Lett.* **12**, 6139 (2012).
- [10] C. Donnelly *et al.*, *Nat. Nanotechnol.* **17**, 136 (2022).
- [11] S. S. P. Parkin *et al.*, *Science* **320**, 190 (2008).
- [12] I. Mönch *et al.*, *ACS Nano* **5**, 7436 (2011).
- [13] R. Streubel *et al.*, *J. Appl. Phys.* **129**, 210902 (2021).
- [14] I. Stanković *et al.*, *Nanoscale* **11**, 2521 (2019).